Int. J. Solids Structures, Vol. 17, No. 12, pp. 1113–1134, 1981
Printed in Great Britain.

0020-7683/81/121113-22$02.00/0
Pergamon Press Ltd.

THE EMERGENCE OF SHEAR BANDS IN PLANE STRAIN

R. ABEYARATNE† and N. TRIANTAFYLLIDIS‡
Brown University, Providence, RI 02912, U.S.A.

(Received 7 August 1980; in revised form 20 February 1981)

Abstract—In this paper, we examine the effect of a slight material imperfection on the deformation field in an otherwise homogeneous body subjected to a plane bi-axial stretch at infinity. Both hyper-elastic and hypo-elastic materials are considered, with the constitutive equations assumed to be such that the governing equilibrium equations lose ellipticity at some strain level. A straightforward regular perturbation analysis is performed and attention is focussed on the features of the first order terms. It is found that the effect of the imperfection is negligible at small values of the applied load. As the load increases, the imperfection more or less abruptly gets "activated" and causes a rapid concentration of strain within certain narrow bands—shear bands—passing through the imperfection. In order to estimate the accuracy of the linearized analysis, a finite element solution of the nonlinear problem is also carried out and results are compared.

INTRODUCTION

A common observation in certain highly deformed ductile solids is that a smoothly varying deformation field more or less abruptly gives way to one which involves narrow bands of highly localized shear deformation (shear bands). Often, the formation of shear bands leads to fracture along these lines of intense shearing so that localization may then be viewed as being a precursor to rupture. The formation of Lüders bands in metals[1] is a well-known example of this phenomenon.

Recently, considerable effort has been directed towards the theoretical understanding and modelling of this phenomenon. Analytical studies have been carried out by Hill[2], Thomas[3] and more recently by Rudnicki and Rice[4], Rice[5] for inelastic materials and by Knowles and Sternberg[6] for nonlinearly elastic ones. In all of these works, the pre-localization field is homogeneous and it is found that a bifurcation mode involving a localized shear band is first possible when the system of governing differential equations loses ellipticity. Because of the uniformity of the deformation field prior to localization, shear bands appear suddenly and the analysis leaves undetermined their exact location in the body.

Experimental observations suggest that "imperfections"—inherent non-uniformities in the material properties—play an important role in the initiation and growth of localized shear zones. In the case of polycrystalline aggregates, shear bands often start appearing at regions of imperfection in the material, such as voids, second phase particles or other inclusions, and then propagate into the rest of the body, usually along grain boundaries[7]. So far only some very elementary steps have been taken in order to account for the role of imperfections.

Recently however, Tvergaard *et al.*[8] completed a very interesting numerical study of the plane strain tension test. There it is shown how a small geometric imperfection in the form of a thickness variation in the specimen can be the "triggering mechanism" which instigates the appearance of shear bands.

In this paper, we attempt to provide an analytical explanation, at least of the qualitative features, of the emergence of shear bands in a ductile metal which is subjected to large plastic deformations under conditions of plane strain. In particular, we examine the role played by a material imperfection in the initiation of shear bands. More specifically, we consider an infinite, isotropic, incompressible body whose material properties are homogeneous outside a certain bounded region of the body; the properties inside this region are slightly different to those outside. At infinity, we suppose that the deformation state is one of uniform bi-axial stretch. Our interest lies in examining the features of the deformation field and how they vary with the applied stretch at infinity.

Classical smooth yield surface models of plasticity theory have been found to predict unrealistically high strain-levels for the onset of shear bands. Furthermore, investigations on the stability of plastic flow against shear localization indicates that the critical conditions are

†Materials Research Laboratory.
‡Division of Engineering.

very sensitive to deviations from such a model. In particular, the presence of yield surface vertex effects (which are predicted by polycrystalline models[9–11]) brings down the theoretically predicted critical values of strain to more realistic levels. A simple way of taking into account the destabilizing effect of a corner on the yield surface is to use a deformation theory of plasticity. The J_2 deformation theory is the most frequently used for bifurcation calculations at small strain levels. In the case of large strains, there is no unique generalization of this theory. Here, two different generalizations of it will be considered, the finite strain version proposed by Stören and Rice[12] which is in fact a hypo-elastic model (with no associated strain energy density function) and the hyper-elastic model, both having the same uniaxial stress–strain curve.

In the theoretical analysis (and the subsequent numerical calculations), we will assume that the magnitude of the imperfection is sufficiently small so as to ensure that the solution to our problem is always in the total loading regime. Since no unloading occurs in a "perfect" (imperfection-free) body, at least until the loss of ellipticity, such a choice of imperfection amplitude can always be made.

It should be mentioned that in view of the prescribed displacement boundary conditions, geometric instabilities do not occur in the problem under consideration here. Consequently, for the perfect body, there is a unique deformation field associated with any prescribed value of the stretch at infinity, provided that the relevant equations remain elliptic. This is in contrast to the problem studied by Tvergaard *et al.*[8], in which localization is preceded by diffuse necking of the specimen in the elliptic regime.

Making use of the small difference in material properties inside and outside the imperfection, we carry out a regular perturbation analysis of the problem. We focus our attention on the first order terms only and find that they display most of the experimentally observed features discussed previously. In particular, it is seen that the effect of the imperfection on the deformation field is negligibly small until the applied stretch at infinity approaches a certain critical value λ_{cr}. As the applied stretch approaches this value, we observe that the strains rapidly concentrate along two directions emanating from the imperfection. The "speed" with which these localized zones propagate through the body increases dramatically as the critical applied stretch is approached. This critical value of the applied stretch λ_{cr} is in fact the value of the prescribed stretch at which a bi-axially stretched perfect body loses ellipticity. The directions of localization are the associated characteristic directions.

Experiments conducted by Anand and Spitzig[13] on aged maraging steel indeed show that internal shear bands start forming when the plastic strain reaches a certain critical level. Increasing the strains beyond this value causes these zones to rapidly propagate through the body (and multiply) until fracture.

Despite the good qualitative agreement between the predictions of our model and observations, we find that the regular perturbation analysis is not uniformly valid with respect to the applied stretch at infinity. Consequently, one would not expect the quantitative results, especially when the applied stretch is close to λ_{cr}, to be reliable. In order to estimate the range of validity of the linearized analysis, a finite element solution of the nonlinear problem posed here was undertaken. Surprisingly, we find that the numerical results compare remarkably well with the perturbation solution, even at values of the applied stretch very close to the critical one.

1. PROBLEM FORMULATION

We consider an isotropic, incompressible body undergoing deformation under conditions of plane strain. Our rectangular cartesian reference frame will be oriented such that the cross-section of the body occupies the entire (z_1, z_2)-plane and all field quantities are independent of the z_3-coordinate.

The body is subjected to a biaxial stretch at infinity parallel to the z_1- and z_2-axes and the resulting deformation is described by

$$y_\alpha = y_\alpha(z) = z_\alpha + u_\alpha(z), \tag{1.1}^\dagger$$

†Greek subscripts take the values 1, 2 and repeated subscripts are summed over this range.

where y is the current position vector of a material point which was located at z in the reference configuration and u is its displacement vector.

A Lagrangian formulation of the field equations is adopted and cartesian coordinates are used in the subsequent analysis. Here, this formulation is briefly outlined. For more details the interested reader is referred to Green and Zerna[14] and Budiansky[15].

The following kinematical quantities are needed: the deformation gradient tensor F whose components are given by

$$F_{\alpha\beta} = y_{\alpha|\beta} = \delta_{\alpha\beta} + u_{\alpha|\beta}, \tag{1.2†}$$

the right Cauchy–Green tensor C with components

$$C_{\alpha\beta} = F_{\gamma\alpha}F_{\gamma\beta} \tag{1.3}$$

and the Lagrangian strain tensor E with components

$$E_{\alpha\beta} = \tfrac{1}{2}(C_{\alpha\beta} - \delta_{\alpha\beta}). \tag{1.4}$$

Incompressibility implies that

$$\det(F_{\alpha\beta}) = 1. \tag{1.5}$$

The two fundamental invariants of C are

$$I = C_{\alpha\alpha} = \lambda_1^2 + \lambda_2^2, \quad J = [\det(C_{\alpha\beta})]^{1/2} = \lambda_1\lambda_2, \tag{1.6}$$

where λ_1, λ_2 are the stretch ratios.

In view of (1.5) we have

$$\lambda_1\lambda_2 = 1. \tag{1.7}$$

If s is the (symmetric) second Piola-Kirchoff stress tensor‡ accompanying the deformation at hand, the equilibrium equations in the reference configuration are

$$(F_{\alpha\gamma}s_{\gamma\beta})_{|\beta} = 0. \tag{1.8}$$

For the complete formulation of the problem, the constitutive equations are needed. The two constitutive laws to be employed are, as discussed in the introduction, a nonlinear elastic relation and the Stören and Rice[12] model.

1.1 *Hyper-elastic material*

Here, the unloaded configuration will be used as the reference one. Letting X denote the position vector of a material point in the unloaded configuration, we take $z = X$. Consequently, in view of the applied bi-axial stretch at infinity we have

$$\left.\begin{aligned} y_1 &= \lambda_0 X_1 + 0(R^{-1}), \\ y_2 &= \lambda_0^{-1} X_2 + 0(R^{-1}), \end{aligned}\right\} \text{as } R = |X| \to \infty, (\lambda_0 \geq 1), \tag{1.9}$$

where λ_0 is the applied stretch at infinity (in the X_1-direction).

Suppose that the body is elastic and that it possesses a potential W representing the strain energy density per unit undeformed volume. Since our attention is restricted exclusively to plane, volume-preserving deformations, W may be taken to be a function of the invariant I (see 1.6) and X only, $W = W(I, X)$. The in-plane components of the second Piola–Kirchoff stress

†A vertical stroke followed by a subscript denotes differentiation with respect to the corresponding z-coordinate.

‡The second Piola–Kirchoff stress tensor s is related to the Cauchy (true) stress σ by $\sigma = (\det F)^{-1}FsF^T$.

are now given by

$$s_{\alpha\beta} = 2W'(I, X)\delta_{\alpha\beta} - pC^{-1}_{\alpha\beta}, \tag{1.10}$$

where $W'(I, X) = \partial W(I, X)/\partial I$, $p(X)$ is a scalar (pressure) field arising because of the incompressibility constraint and C^{-1} is the inverse of the right Cauchy–Green tensor C defined by (1.3). We find from (1.3), (1.5), (1.8) and (1.10) that

$$\frac{\partial}{\partial X_\beta}(2W'(I, X)F_{\alpha\beta}) - \frac{\partial p}{\partial X_\beta} F^{-1}_{\beta\alpha} = 0. \tag{1.11}$$

Equation (1.11) together with the incompressibility condition (1.5) constitute the governing system of equations. They are three scalar equations involving the three functions $y_\alpha(X)$, $p(X)$.

In this paper we consider a class of elastic materials whose strain energy density function W conforms to the following requirements:

(i)
$$W = W(I, X) = W_0(I) + \bar{\xi}\bar{W}(I, X), \quad (\bar{\xi} \neq 0), \tag{1.12a}$$

where $\bar{W}(I, \cdot) \equiv 0$ in $R^2 - D$, $\bar{W}(I, \cdot) \neq 0$ in D.

(ii)
$$W_0'(I) > 0 \quad \text{for} \quad I \geq 2. \tag{1.12b}$$

(iii) There exists a number k_{cr} (>0) such that

$$\begin{aligned} \frac{\partial}{\partial k}\{2kW_0'(2+k^2)\} &> 0 \quad \text{for} \quad 0 \leq k < k_{cr}, \\ &= 0 \quad \text{for} \quad k = k_{cr}. \end{aligned} \tag{1.12c}$$

In eqn (1.12a) $\bar{\xi}$ is a constant and $\bar{W}(I, \cdot)$ is a sufficiently smooth function whose support is the bounded region D. Accordingly, (1.12a) describes an elastic body which is homogeneous everywhere in $R^2 - D$ (see Fig. 1). We will refer to D as the "region of imperfection" or simply the "imperfection". When $\bar{\xi} = 0$, the body is called "perfect". The condition (1.12b) is motivated on physical grounds: it ensures that the secant modulus of the perfect material in simple shear is always positive. The final condition (1.12c) is a statement concerning the character of the system of partial differential equations (1.5), (1.11). It has been shown in[16] that this system is *elliptic* at a solution $y_\alpha(X)$, $p(X)$ and at a point X if and only if

$$\frac{\partial}{\partial k}\{2kW'(2+k^2, X)\} > 0, \; k = (I-2)^{1/2}. \tag{1.13†}$$

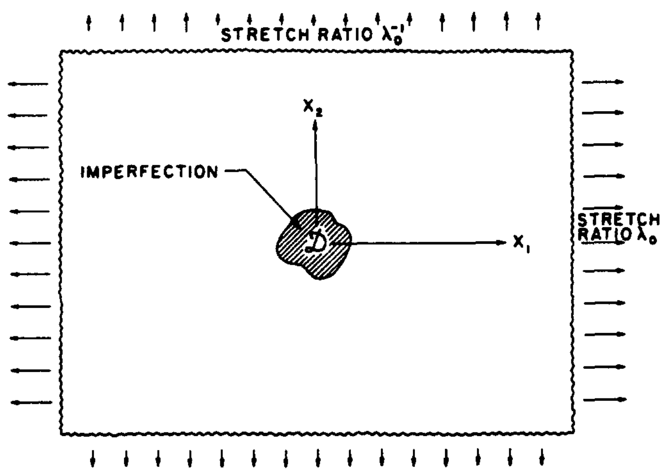

Fig. 1.

†The results in[16] are established for a homogeneous material but may be readily generalized. A physical interpretation of this condition is also given there.

Equation (1.12c) indicates that for sufficiently small strains (i.e. small values of I-2) the perfect material is elliptic and that ellipticity is lost at some critical strain level.

We may now pose the following problem: given an elastic body whose strain energy density W conforms to (1.12), we wish to determine a solution $y_\alpha(X)$, $p(X)$ to (1.2), (1.5) and (1.11) subject to the conditions (1.9) at infinity, when the applied stretch λ_0 is prescribed.

In the particular case of a perfect (imperfection-free) body, the unique solution to this problem is $y_1 = \lambda_0 X_1$, $y_2 = \lambda_0^{-1} X_2$, $p =$ constant, for all λ_0 satisfying the ellipticity condition $\lambda_0 < \lambda_{cr}$ where $\lambda_{cr}^2 + \lambda_{cr}^{-2} - 2 = k_{cr}^2$.

We will illustrate the various features of the perturbation solution obtained in the next section by considering a specific strain-energy density function. For this purpose we consider a material whose uniaxial stress–strain response is described by

$$\frac{\sigma}{\sigma_y} = \frac{\epsilon}{\epsilon_y} \quad \text{for} \quad \epsilon \le \epsilon_y,$$

$$\left(\frac{\sigma}{\sigma_y}\right)^m = \frac{\epsilon}{\epsilon_y} \quad \text{for} \quad \epsilon \ge \epsilon_y, \tag{1.14}$$

where σ is the applied (true) stress and ϵ is the natural strain ($\epsilon = \ln \lambda$). The Young's modulus is $E = \sigma_y/\epsilon_y$ and the constant m is the hardening exponent. Such a piecewise power law description of material response is commonly used in plasticity theory, wherein ϵ_y and σ_y represent the yield strain and stress in uniaxial tension or compression.

A three dimensional elastic potential $W(\lambda_1, \lambda_2, \lambda_3)$ compatible with (1.14) is

$$W(\lambda_1, \lambda_2, \lambda_3) = \begin{cases} \dfrac{E}{2}\epsilon_e^2, & 0 \le \epsilon_e \le \epsilon_y, \\[2ex] \dfrac{m}{m+1} E\epsilon_y^2 \left(\dfrac{\epsilon_e}{\epsilon_y}\right)^{(m+1)/m} + \left(\dfrac{1-m}{1+m}\right)\dfrac{E}{2}\epsilon_y^2, & \epsilon_e \ge \epsilon_y, \end{cases} \tag{1.15a}$$

where the equivalent strain ϵ_e is given in terms of the principal logarithmic strains ϵ_i by

$$\epsilon_e = \frac{2}{3}(\epsilon_1^2 + \epsilon_2^2 + \epsilon_3^2 - \epsilon_1\epsilon_2 - \epsilon_2\epsilon_3 - \epsilon_3\epsilon_1)^{1/2}, \tag{1.15b}$$

$$\epsilon_i = \ln \lambda_i. \tag{1.15c}$$

In order to model the imperfection, we take

$$E = E_0 + \bar{E}(\bar{\xi}, X), \quad \sigma_y = \sigma_y^0, \quad \epsilon_y = \sigma_y^0/E, \tag{1.15d}$$

where $\bar{E}(\bar{\xi}, \cdot)$ is a function with support D, $\bar{E}(0, X) = 0$ and σ_y^0 is a constant. It can be verified that this material conforms to the ellipticity condition (1.12c).

1.2 *Hypo-elastic material*

The Stören and Rice version of the J_2 deformation theory is a hypo-elastic constitutive law, which is in general, history dependent. Consequently, the rate form of the field equations must be used. Throughout this paper we define the rate of a field quantity, denoted by $(\dot{\cdot})$, to be its derivative with respect to some monotonically increasing parameter with the reference position z held fixed. Here we choose λ_0, the applied stretch at infinity in the X_1 direction, as such a history parameter.

Differentiation of (1.8) with respect to the history parameter, leads to the rate form of the equilibrium equations

$$(\dot{s}_{\alpha\beta} + s_{\gamma\beta}\dot{u}_{\alpha|\gamma} + \dot{s}_{\gamma\beta}u_{\alpha|\gamma})_{|\beta} = 0. \tag{1.16}$$

Similarly, from the incompressibility condition (1.5) we find

$$\dot{u}_{\alpha|\alpha} + \tfrac{1}{2}\,\epsilon_{\alpha\beta}\epsilon_{\gamma\delta}(u_{\alpha|\gamma}\dot{u}_{\beta|\delta} + \dot{u}_{\alpha|\gamma}u_{\beta|\delta}) = 0. \tag{1.17}$$

The constitutive equation for an incompressible hypo-elastic material, under plane strain conditions, takes the form

$$\dot{s}_{\alpha\beta} = L_{\alpha\beta\gamma\delta}\dot{E}_{\gamma\delta} - \dot{p}C^{-1}_{\alpha\beta}, \tag{1.18}$$

(e.g. see[17]) where C is the right Cauchy–Green deformation tensor while $\dot{E}$ is the rate of the Lagrangian strain E and has components

$$\dot{E}_{\alpha\beta} = \tfrac{1}{2}(\dot{u}_{\alpha|\beta} + \dot{u}_{\beta|\alpha} + \dot{u}_{\gamma|\alpha}u_{\gamma|\beta} + u_{\gamma|\alpha}\dot{u}_{\gamma|\beta}). \tag{1.19}$$

For the Stören and Rice material[12] the components of the incremental moduli tensor L are given by

$$\begin{aligned} L_{\alpha\beta\gamma\delta} = \frac{2}{3}E_s\left[\frac{1}{2}(C^{-1}_{\alpha\gamma}C^{-1}_{\beta\delta} + C^{-1}_{\alpha\delta}C^{-1}_{\beta\gamma}) - \frac{3}{2}\left(1 - \frac{E_t}{E_s}\right)\frac{s'_{\alpha\beta}S'_{\gamma\delta}}{\sigma_e^2}\right] \\ -\frac{1}{2}[C^{-1}_{\alpha\gamma}s_{\beta\delta} + C^{-1}_{\beta\gamma}s_{\alpha\delta} + C^{-1}_{\alpha\delta}s_{\beta\gamma} + C^{-1}_{\beta\delta}s_{\alpha\gamma}], \end{aligned} \tag{1.20}$$

where

$$s'_{\alpha\beta} = s_{\alpha\beta} - \tfrac{1}{2}C^{-1}_{\alpha\beta}C_{\gamma\delta}s_{\gamma\delta}, \quad \sigma_e^2 = \tfrac{3}{2}C_{\alpha\gamma}C_{\beta\delta}s_{\alpha\beta}s_{\gamma\delta}. \tag{1.21}$$

Here E_t and E_s are the tangent and secant moduli respectively of the uniaxial true stress–natural strain curve at a stress level equal to the equivalent stress σ_e.

Without loss of generality the imperfection in this case is considered to be of the form:

$$q(z) = q_0 + \bar{\xi}\bar{q}(z) \tag{1.22}$$

where q stands for any material property. In analogy with (1.12a), $\bar{q}$ is a function of bounded support D. It is understood that E_s and E_t have an explicit dependence on q. When the uniaxial stress–strain curve is taken to be the same piecewise power law (1.14) that we assumed for the hyper-elastic material, we find the following expressions for E_t and E_s:

$$\begin{aligned} E_t = E \quad \text{for} \quad \sigma_e \le \sigma_y,\ E_t = \frac{E}{m}\left(\frac{\sigma_e}{\sigma_y}\right)^{1-m} \quad \text{for} \quad \sigma_e > \sigma_y, \\ E_s = E \quad \text{for} \quad \sigma_e \le \sigma_y,\ E_s = E\left(\frac{\sigma_e}{\sigma_y}\right)^{1-m} \quad \text{for} \quad \sigma_e > \sigma_y, \end{aligned} \tag{1.23}$$

The governing (nonlinear) problem for the imperfect Stören and Rice hypo-elastic body is then completely posed if one supplements equations (1.16)–(1.22) with the requirement that the asymptotic behavior at infinity of the displacement field u is to be given by (1.9).

Here also, it can be easily verified that in the case of a perfect body, i.e. $\bar{\xi} = 0$, the solution to the above problem describes a state of homogeneous strain (and stress). In this case the principal axes of strain at any material point remain fixed with respect to the material (as the history parameter varies) and therefore, as discussed by Stören and Rice[12] their constitutive model is path independent. Consequently, the final state of stress here is identical to that of the perfect elastic body (for the same value of λ_0).

2. REGULAR PERTURBATION PROBLEM FORMULATION

2.1 *Hyper-elastic material*

As discussed in the previous section, the deformation of the perfect body, $\bar{\xi}=0$, is a purely homogeneous one, with the current position of a material point x being related to its reference position X by

$$x_1=\lambda_0 X_1,\ x_2=\lambda_0^{-1}X_2. \tag{2.1}$$

When the magnitude of the imperfection is small, $|\bar{\xi}|\ll 1$, it is reasonable to expect that the current position y will not be significantly different from the position x.

In this paper we restrict our attention to the case of a *small* imperfection amplitude and perform a regular perturbation analysis of the problem using $\bar{\xi}$ as the "small parameter."

Accordingly, we assume that the current position $y(X,\bar{\xi})$ and the pressure $p(X,\bar{\xi})$ admit the following asymptotic representations:

$$\begin{aligned} y_1&=\lambda_0X_1+\bar{\xi}\bar{u}_1(X)+o(\bar{\xi}),\\ y_2&=\lambda_0^{-1}X_2+\bar{\xi}\bar{u}_2(X)+o(\bar{\xi}),\\ p&=p_0+\bar{\xi}\bar{p}(X)+o(\bar{\xi}), \end{aligned} \tag{2.2}$$

as $\bar{\xi}\to 0$. Throughout this paper, quantities associated with the uniform field (the zeroth order terms) will have a superscript or subscript (0) while the first order perturbation terms will be surmounted by a (‒). Corresponding expansions for the various field quantities introduced in the previous section may now be deduced.

On making use of (2.2), the incompressibility condition (1.5) yields $\lambda_0^{-1}\partial\bar{u}_1/\partial X_1+\lambda_0\,\partial\bar{u}_2/\partial X_2=0$ to leading order. At this point, it is convenient to change independent variables from (X_1, X_2) to (x_1, x_2) where x is defined by (2.1). For notational convenience we will use the same symbols to denote a function of x and the corresponding function of X. A comma followed by a subscript will indicate differentiation with respect to the corresponding x-coordinate. The incompressibility condition now takes the form $\bar{u}_{\alpha,\alpha}=0$ from which it follows that $\bar{u}(x)$ admits the representation

$$\bar{u}_\alpha=\epsilon_{\alpha\beta}\psi_{,\beta} \tag{2.3}$$

where the displacement potential $\psi(x)$ is any sufficiently smooth scalar-valued function.

The displacement equations of equilibrium (1.11) may be similarly evaluated to leading order on making use of (1.12a) and (2.2). The pressure term $\bar{p}$ may be eliminated from the resulting two equations which, after making use of (2.3), leads to

$$\left(\mu+\frac{\sigma}{2}\right)\psi_{,1111}+2(2\mu^*-\mu)\psi_{,1122}+\left(\mu-\frac{\sigma}{2}\right)\psi_{,2222}=g, \tag{2.4}$$

where we have set

$$\begin{aligned} \mu&=(\lambda_0^2+\lambda_0^{-2})W_0'(I^0),\quad \sigma=2(\lambda_0^2-\lambda_0^{-2})W_0'(I^0),\\ \mu^*&=(\lambda_0^2+\lambda_0^{-2})W_0'(I^0)+(\lambda_0^2-\lambda_0^{-2})^2W_0''(I^0),\\ g&=2(\lambda_0^{-2}-\lambda_0^2)\bar{W}'_{,12}(I^0,x). \end{aligned} \tag{2.5}$$

In view of (1.9), (2.2) and (2.3) we will require that at infinity

$$\psi_{,\alpha}=O(r^{-1})\ \text{as}\ r=|x|\to\infty. \tag{2.6}$$

The l.h.s. of (2.4) is identical to eqn (3.3) obtained by Hill and Hutchinson[18]. This coincidence is hardly surprising, since they both describe incremental equilibrium from the same uniform reference state of plane strain of an incompressible, isotropic body. Following Hill and Hutchinson[18], the constants μ and μ^* may be interpreted as being the shearing moduli (of the perfect body) associated with an infinitesimal simple shear superposed on a pure homogeneous deformation; μ for shearing parallel to the principal axes and μ^* for shearing at 45° to them. Moreover, σ is the difference between the principal (in-plane) Cauchy stresses.

The differential equation (2.4) is said to be *elliptic*, *parabolic*, or *hyperbolic* according to whether there are exactly no, two, or four real values of n_1/n_2 which satisfy its characteristic equation

$$\left(\mu+\frac{\sigma}{2}\right)n_1^4+2(2\mu^*-\mu)n_1^2n_2^2+\left(\mu-\frac{\sigma}{2}\right)n_2^4=0. \tag{2.7}$$

In view of (1.12b) and (2.5) it follows that the coefficients of eqn (2.4) obey

$$\mu+\frac{\sigma}{2}>0,\ \mu-\frac{\sigma}{2}>0, \tag{2.8}$$

Consequently, (2.4) can be shown to be elliptic (everywhere in R^2) if and only if

$$2\mu^*-\mu+\sqrt{\mu^2-\frac{\sigma^2}{4}}>0. \tag{2.9a}$$

From (2.8) it also follows that (2.4) can never be parabolic (see Hill and Hutchinson[18]).

Substituting for μ, μ^* and σ from (2.5) and making use of (1.12b), shows that (2.9a) is equivalent to

$$\frac{\partial}{\partial k}\{2kW_0'(2+k^2)\}>0,\ k=(I^0-2)^{1/2}. \tag{2.9b}$$

It therefore follows from (2.9b) and (1.13) that at a given value of the applied stretch λ_0, the *linear* differential equation governing the displacement potential ψ (for the *imperfect* body) is elliptic if and only if the *nonlinear* equations (1.5), (1.11) governing the equilibrium of the *perfect* body (at the same value of λ_0) are also elliptic.

For the class of materials defined through (1.12) considered here, there exists a critical value of the applied stretch, λ_{cr}, such that (2.4) is elliptic when $1<\lambda_0<\lambda_{cr}$ and hyperbolic when $\lambda_0=\lambda_{cr}$. When $\lambda_0=\lambda_{cr}$ there are two† families of characteristics, $x_1\tan\theta_{cr}\pm x_2=$ constant, associated with this equation and the characteristic angle (in the current configuration) θ_{cr} obeys

$$\tan\theta_{cr}=\lambda_{cr}^{-1}. \tag{2.10}$$

In the particular case of the power law material (1.15), we find from (2.9) that the value of λ_{cr} is given by the unique (> 1) root of

$$(\lambda_{cr}^2+1)/(\lambda_{cr}^2-1)=m\ln\lambda_{cr}. \tag{2.11}$$

In this paper we will *restrict our attention* to values of λ_0 which are strictly less than λ_{cr}. Consequently, the linear differential equation, (2.4), and also the nonlinear equations associated with the perfect body, remain elliptic throughout our discussions. On the other hand, one would anticipate that the nonlinear equations governing the equilibrium of the imperfect body *will* lose ellipticity, locally in the vicinity of the imperfection, at a value of λ_0 somewhat smaller than λ_{cr}.

†The four real values of n_1/n_2 satisfying (2.7) in this case appear in two distinct pairs.

2.2 *Hypo-elastic material*

For simplicity, in this case we choose as reference configuration the configuration assumed by the perfect body when it is subjected to stretches identical to those applied at infinity to the imperfect body.† Accordingly, here we take $z = x$ where the spatial variables x_1, x_2 were introduced in (2.1). It is understood that all field quantities are functions of x_1, x_2 and the history parameter λ_0.

Again, we assume that the magnitude of the imperfection is small, $|\bar{\xi}| \ll 1$, and take the displacements and stresses to be of the form

$$u_\alpha \sim 0 + \bar{\xi}\bar{u}_\alpha,\ \dot{u}_\alpha \sim \dot{u}^0_\alpha + \bar{\xi}\dot{\bar{u}}_\alpha,\ s_{\alpha\beta} \sim s^0_{\alpha\beta} + \bar{\xi}\bar{s}_{\alpha\beta} \tag{2.12}$$

as $\bar{\xi} \to 0$. The zeroth order terms describe the perfect body and, as remarked at the end of Section 1.2, are identical to the corresponding terms for the hyper-elastic material. In particular, we have

$$\begin{aligned} &\dot{u}^0_1 = \lambda_0^{-1}x_1, \quad \dot{u}^0_2 = -\lambda_0^{-1}x_2, \\ &s^0_{12} = s^0_{21} = 0, \quad s^0_{11} - s^0_{22} = \sigma. \end{aligned} \tag{2.13}$$

On making use of (2.12), the (rate form of the) incompressibility condition (1.17) may be evaluated and gives $(\dot{\bar{u}}_\beta - \dot{u}^0_{\alpha,\beta}\bar{u}_\alpha)_{,\beta} = 0$ to leading order. Consequently there exists a function ψ such that

$$\dot{\bar{u}}_\beta - \dot{u}^0_{\alpha,\beta}\bar{u}_\alpha = \epsilon_{\beta\gamma}\psi_{,\gamma}. \tag{2.14}$$

Similarly, the incremental equilibrium equations (1.16) and the constitutive relation (1.18) may also be evaluated to leading order. Combining the resulting equations, eliminating the pressure term and utilizing (2.14) leads to

$$\left(\mu + \frac{\sigma}{2}\right)\psi_{,1111} + 2(2\mu^* - \mu)\psi_{,1122} + \left(\mu - \frac{\sigma}{2}\right)\psi_{,2222} = g \tag{2.15}$$

where the r.h.s. is given by

$$\begin{aligned} g = -\Bigg\{ &\left[2L^0_{\alpha\beta\gamma\delta}\delta_{\epsilon\zeta} + \left.\frac{\partial L_{\alpha\beta\zeta\delta}}{\partial u_{\epsilon,\gamma}}\right|_0 + L^0_{\gamma\beta\zeta\delta}\delta_{\alpha\epsilon} + s^0_{\beta\gamma}\delta_{\alpha\delta}\delta_{\epsilon\zeta}\right]\dot{u}^0_{\zeta,\delta}\bar{u}_{\epsilon,\gamma\beta\theta} \\ &+ \left[\left.\frac{\partial L_{\alpha\beta\gamma\delta}}{\partial s_{\epsilon\zeta}}\right|_0 + \delta_{\epsilon\gamma}\delta_{\beta\zeta}\delta_{\alpha\delta}\right]\dot{u}^0_{\delta,\gamma}\bar{s}_{\epsilon\zeta,\beta\theta} + \left.\frac{\partial L_{\alpha\beta\gamma\delta}}{\partial q}\right|_0 \bar{q}_{,\beta\theta}\dot{u}^0_{\gamma,\delta}\Bigg\}\epsilon_{\alpha\theta} \end{aligned} \tag{2.16}$$

and we have set

$$\mu = \tfrac{1}{3}E^0_s, \quad \mu^* = \tfrac{1}{3}E^0_t. \tag{2.17}$$

As in the previous sub-section μ and μ^* are the incremental shear moduli of the material.

The l.h.s. of (2.15) is, as expected, identical to the left hand side of (2.4) since it also represents the incremental equilibrium equation around a uniform state of plane strain of an incompressible, initially isotropic material. *In contrast* to (2.4) however, the r.h.s. of (2.15) involves the ***unknown*** quantities $\bar{u}$ and $\bar{s}$.

As discussed by Hill and Hutchinson[18], for a general hypo-elastic material all three states (elliptic, parabolic and hyperbolic) are possible. For the particular power-law material described previously (1.14), the study of the roots of the characteristic equation (2.7) gives the following

†The resulting formulation is commonly referred to as being an updated Lagrangian one.

results: Equation (2.15) is

$$\left.\begin{array}{ll}\text{elliptic when} & 1 \le \lambda_0 < \exp(0.5),\\ \text{parabolic when} & \lambda_0 \ge \exp(0.5),\end{array}\right\} \text{ for } m < 2$$

$$\left.\begin{array}{ll}\text{elliptic when} & 1 \le \lambda_0 < \exp(\sqrt{m-1}/m),\\ \text{hyperbolic when} & \exp\sqrt{m-1/m}) \le \lambda_0 < \exp(0.5),\\ \text{parabolic when} & \exp(0.5) < \lambda_0.\end{array}\right\} \text{ for } m \ge 2. \tag{2.18}$$

The characteristic directions at the instant of loss of ellipticity are $x_2 \pm (\tan\theta_{cr})x_1 = \text{constant}$ where the angle θ_{cr} is given by

$$\theta_{cr} = \begin{cases} 0 \quad \text{for} \quad m \le 2, \\ \tan^{-1}\left[\dfrac{m-2}{m+2\sqrt{m-1}}\right]^{1/2} \quad \text{for} \quad m > 2. \end{cases} \tag{2.19}$$

Here again, the analysis is restricted to the case $\lambda_0 < \lambda_{cr}$ where λ_{cr} is the critical value of the applied stretch at which the perfect material first loses ellipticity:

$$\lambda_{cr} = \begin{cases} \exp(0.5) \quad \text{for} \quad m \le 2. \\ \exp\left(\dfrac{\sqrt{m-1}}{m}\right) \quad \text{for} \quad m > 2. \end{cases} \tag{2.20}$$

3. REGULAR PERTURBATION PROBLEM. SOLUTION

A formal solution to the linear partial differential equation (2.4) or (2.15) may be obtained as follows. Letting $g(x_1, x_2)$ denote the r.h.s. of either of these equations, we seek a solution in the (convolution) form

$$\psi(x_1, x_2) = \int_{-\infty}^{\infty}\int_{-\infty}^{\infty} G(x_1 - \omega_1, x_2 - \omega_2) g(\omega_1, \omega_2)\, d\omega_1\, d\omega_2. \tag{3.1}\dagger$$

The function G then satisfies

$$\left(\mu + \frac{\sigma}{2}\right) G_{,1111} + 2(2\mu^* - \mu) G_{,1122} + \left(\mu - \frac{\sigma}{2}\right) G_{,2222} = \delta(x_1)\delta(x_2) \tag{3.2}$$

where $\delta(\cdot)$ denotes Dirac's delta distribution, and G is to be suitably restricted at infinity.

A solution to (3.2) may be obtained through a generalized Fourier transform (see Lighthill[15]) or by appropriating the results in Gel'fand and Shilov[20] Section 6.1:

$$G(x_1, x_2) = \frac{1}{(4\pi)^2}\int_0^{2\pi} \frac{(x_1\cos\phi + x_2\sin\phi)^2 \ln(x_1\cos\phi + x_2\sin\phi)^2}{(\mu + \sigma/2)\cos^4\phi + 2(2\mu^* - \mu)\cos^2\phi\sin^2\phi + (\mu - \sigma/2)\sin^4\phi}\, d\phi. \tag{3.3}$$

In view of the *ellipticity* of eqns (2.4) and (2.15), the denominator of (3.3) does not vanish. The function G is in fact an ordinary function and has continuous first derivatives on R^2.

The integral appearing in (3.3) may be evaluated by contour integration and leads to the following results: If the roots of the polynomial

$$\left(\mu - \frac{\sigma}{2}\right) z^4 + 2(2\mu^* - \mu) z^2 + \left(\mu + \frac{\sigma}{2}\right) = 0 \tag{3.4}$$

†One can define physically meaningful function spaces V and V' such that for every g in V' there exists a unique solution ψ in V. In particular, the function g associated with the specific imperfection (3.17), (3.18) used subsequently, and the corresponding "solution" ψ that we find, *do* belong to V' and V. The authors are indebted to Prof. C. Dafermos for this observation.

consist of two complex conjugate pairs, then

$$G(x_1,x_2)=\frac{1}{16\pi\beta(\mu-\sigma/2)}\left\{\frac{1}{2(\alpha^2+\beta^2)}[((x_1+x_2\alpha)^2+(x_2\beta)^2)\ln((x_1+x_2\alpha)^2+(x_2\beta)^2)\right.$$
$$+((x_1-x_2\alpha)^2+(x_2\beta)^2)\ln((x_1-x_2\alpha)^2+(x_2\beta)^2)]+\frac{x_1x_2\beta^2}{\alpha(\alpha^2+\beta^2)}$$
$$\left.\ln\left(\frac{(x_1+x_2\alpha)^2+(x_2\beta)^2}{(x_1-x_2\alpha)^2+(x_2\beta)^2}\right)+\frac{\beta}{\alpha}\left(x_2^2-\frac{x_1^2}{\alpha^2+\beta^2}\right)\tan^{-1}\left(\frac{2\alpha\beta x_2^2}{x_1^2-\alpha^2x_2^2+\beta^2x_2^2}\right)\right\}. \tag{3.5}$$

Here, the positive numbers α and β are given by

$$\alpha=\left[\frac{1}{2}\left\{\left(\frac{\mu+(\sigma/2)}{\mu-(\sigma/2)}\right)^{1/2}-\frac{2\mu^*-\mu}{\mu-(\sigma/2)}\right\}\right]^{1/2},$$
$$\beta=\left[\frac{1}{2}\left\{\left(\frac{\mu+(\sigma/2)}{\mu-(\sigma/2)}\right)^{1/2}+\frac{2\mu^*-\mu}{\mu-(\sigma/2)}\right\}\right]^{1/2}, \tag{3.6†}$$

so that $\alpha+i\beta, \alpha-i\beta, -\alpha+i\beta, -\alpha-i\beta$ are the roots of the polynomial (3.4). In view of (2.8), (2.9a) any hyper-elastic material falls into this category, as do also certain hypo-elastic materials (in particular the power-law materials considered here with hardening exponent $m>2$).

In the case where (3.4) has two pairs of purely imaginary conjugate roots (which is the case for a power law hypo-elastic material with $1\le m\le 2$) one finds

$$G(x_1,x_2)=\frac{1}{8\pi(\alpha^2-\beta^2)(\mu-(\sigma/2))}\left[4x_1x_2\left(\tan^{-1}\frac{\alpha x_2}{x_1}-\tan^{-1}\frac{\beta x_2}{x_1}\right)\right.$$
$$\left.+\frac{1}{\beta}(x_1^2-\beta^2x_2^2)\ln(x_1^2+\beta^2x_2^2)-\frac{1}{\alpha}(x_1^2-\alpha^2x_2^2)\ln(x_1^2+\alpha^2x_2^2)\right], \tag{3.7}$$

where the positive numbers α and β are now found to be

$$\alpha=\left[\frac{2\mu^*-\mu}{\mu-(\sigma/2)}-\left\{\left(\frac{2\mu^*-\mu}{\mu-(\sigma/2)}\right)^2-\frac{\mu+(\sigma/2)}{\mu-(\sigma/2)}\right\}^{1/2}\right]^{1/2},$$
$$\beta=\left[\frac{2\mu^*-\mu}{\mu-(\sigma/2)}+\left\{\left(\frac{2\mu^*-\mu}{\mu-(\sigma/2)}\right)^2-\frac{\mu+(\sigma/2)}{\mu-(\sigma/2)}\right\}^{1/2}\right]^{1/2}, \tag{3.8}$$

and $\pm i\alpha, \pm i\beta$ are the roots of the polynomial (3.4).

In the remainder of this section we discuss some qualitative features of these formulae.

3.1 *Hyper-elastic material*

We note that if the material properties in the imperfection vary (smoothly and) symmetrically with respect to the X_1- and X_2-axes, then $g(x_1,x_2)=-g(x_1,-x_2)=-g(-x_1,x_2)$ on D. Consequently, it can be readily shown from (3.1) and (3.5) that ψ obeys the condition (2.6) at infinity, so that (3.1), (3.5) *does* provide a formal solution to our problem.

In order to exhibit the localization effects predicted by the preceding solution, we will examine the spatial variation of two representative field quantities, viz. the equivalent strain ϵ_e and the shear component E_{12} of the Lagrangian strain.

From (1.6), (1.7), (2.2) and (2.3) we find

$$\epsilon_e\sim\epsilon_e^0+\bar{\xi}\bar{\epsilon}_e=\frac{2}{\sqrt{3}}\lambda_0+\bar{\xi}\frac{2}{\sqrt{3}}\psi_{,12} \tag{3.9}$$

†The reality of the numbers α and β in (3.6) and (3.8) is ensured by the ellipticity of the governing differential equation.

for the equivalent strain ($\epsilon_e = 2|\ln\lambda|/\sqrt{3}$). Using (3.1), (3.5) and (3.9) we find that

$$\bar{\epsilon}_e = \frac{2}{\sqrt{3}}\int_{-\infty}^{\infty}\int_{-\infty}^{\infty} G_{,12}(x_1-\omega_1, x_2-\omega_2)g(\omega_1,\omega_2)\,d\omega_1\,d\omega_2, \tag{3.10}$$

$$G_{,12}(x_1,x_2) = \frac{1}{16\pi\alpha\beta(\mu-\sigma/2)}\ln\left[\frac{(x_1+\alpha x_2)^2+\beta^2x_2^2}{(x_1-\alpha x_2)^2+\beta^2x_2^2}\right]. \tag{3.11}$$

As mentioned previously, our primary interest lies in the examination of the behavior of this solution as the applied stretch at infinity λ_0 approaches the critical value λ_{cr} at which the equation loses ellipticity. For this purpose, we need to determine the dependence of α and β on λ_0 and find from (2.5), (2.9a) and (3.6) that

$$\alpha \to \lambda_{cr}, \quad \beta \to 0 \tag{3.12}$$

as $\lambda_0 \to \lambda_{cr}$. Consequently, the logarithmic term in (3.11) becomes unbounded along the straight lines $x_1 \pm \lambda_{cr}x_2 = 0$ in this limit but remains bounded everywhere else. These lines are in fact the characteristics of eqn (2.4) at the instant of loss of ellipticity.

We therefore expect that as λ_0 is increased and approaches λ_{cr}, the strains concentrate ("*localize*") along two directions passing through the imperfection and parallel to (what are to become) the characteristic directions. Furthermore, calculations performed in specific examples, suggest that this localization of strain is in fact largely confined to values of λ_0 which are very close to λ_{cr}, with negligible strain concentration before that. This is qualitatively in agreement with experimental observations, e.g. Anand and Spitzig[13], wherein shear bands are seen to appear more or less abruptly.

The shear strain E_{12}, which according to (1.6), (1.7) and (2.3) obeys

$$E_{12} \sim E_{12}^0 + \bar{\xi}\bar{E}_{12} = 0 + \frac{\bar{\xi}}{2}(\psi_{,22} - \psi_{,11}), \tag{3.13}$$

can be shown to exhibit these same features.

For purposes of illustration, we present a number of graphs (Figs. 2–13) showing the spatial variation of shear strain in the body. The calculations are performed for a power-law material (1.15) and a particularly simple form of imperfection. The latter is modelled by taking the Young's modulus (1.15d) to be of the form

$$E = E_0(1+\bar{\xi}f(X)), \quad f(X) = [H(X_1+A)-H(X_1-A)][H(X_2+B)-H(X_2-B)]. \tag{3.14}$$

Here A and B are constants and H is the Heaviside step function. The "yield stress" is assumed to be constant throughout the body, $\sigma_y \equiv \sigma_y^0$. It can be shown that the strain energy function (1.12) associated with such a material is

$$W = W_0(I)\left\{1+\frac{\bar{\xi}}{m}f(X)\right\} + 0(\bar{\xi}^2), \tag{3.15}$$

where W_0 is the plane strain version of (1.15a) with $E = E_0$, $\epsilon_y = \epsilon_y{}^0$ and $\sigma_y = \sigma_y{}^0$. This describes a *rectangular imperfection* of undeformed cross-sectional dimensions $2A \times 2B$. The materials outside and inside the imperfection are both homogeneous and of the power-law type (1.14) with the Young's modulus being E_0 and $E_0(1+\bar{\xi})$ respectively.

From (3.9), (3.1), (3.5), (2.5), (3.15), (3.14) and (3.12) we find that in the limit $\lambda_0 \to \lambda_{cr}$, the strains $\bar{\epsilon}_e$ and $\bar{E}_{12}$ become unbounded along the (eight) straight lines which pass through the vertices of the rectangular imperfection and have slopes $\pm\lambda_{cr}^{-1}$.

A pictorial representation of these results is shown in Fig. 2-4. The results are presented relative to the undeformed configuration for a material with hardening exponent $m = 4$, imperfection amplitude $\bar{\xi} = -0.01$ and imperfection dimensions $A/B = 1.685$ ($\simeq \lambda_{cr}$). We note that the characteristic angle (in this configuration) is $\theta_{cr} = \tan^{-1}\lambda_{cr} \simeq 59.3°$.

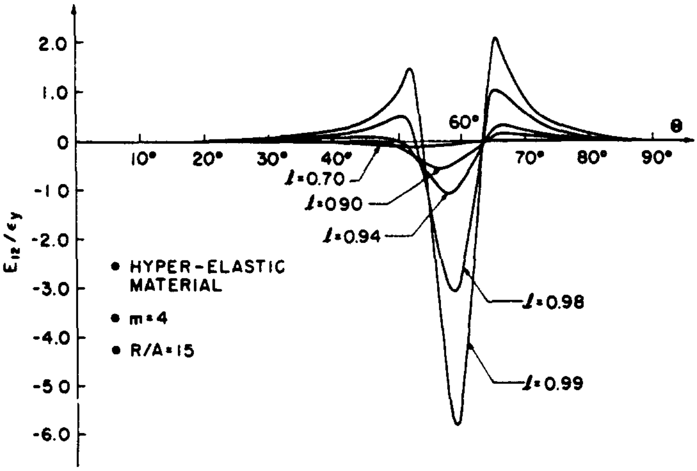

Fig. 2.

Figure 2 shows the angular variation of the (non-dimensional) shear strain E_{12}/ϵ_y along the circular arc of radius $R = 15A$ centered at the origin. The graph is drawn for various values of the prescribed deformation—"load"— l,

$$l = \frac{\lambda_0 - 1}{\lambda_{cr} - 1}. \tag{3.16}$$

(As the applied stretch λ_0 varies from 1 to λ_{cr}, the load l varies from 0 to 1.) We observe that the shear strain is negligibly small when the load is less than about 0.7. As the load level increases, the strain continues to remain small everywhere except in a certain narrow zone in the vicinity of $\theta = 59°$ in which it is no longer insignificant. As the load approaches 1, the strain in this zone concentrates quite dramatically; for example, it almost doubles in value near the peaks when the load increases from 0.98 to 0.99. The three peaks observed are associated with the three characteristics which pass through the vertices of the imperfection and propagate into the first quadrant. (The particular choice of dimensions of the imperfection $A/B = \lambda_{cr}$ is such that there are only three such (distinct) lines instead of the four that exist in general.)

In Fig. 3 we have plotted contours of constant shear strain for $E_{12}/\epsilon_y = -3, -2, 0, +0.07, +0.5, +1$ at a fixed load level $l = 0.98$. In Fig. 4, the constant shear strain contour $E_{12}/\epsilon_y = -2$ is plotted at different load levels $l = 0.8, 0.9, 0.94, 0.96, 0.98$. Both of these graphs show that the effect of the imperfection is felt predominantly along the characteristic directions. The second further indicates that the effect becomes significant only when the applied stretch λ_0 takes on values close to λ_{cr}. Results for various other cases which are plotted later, also bear out these observations.

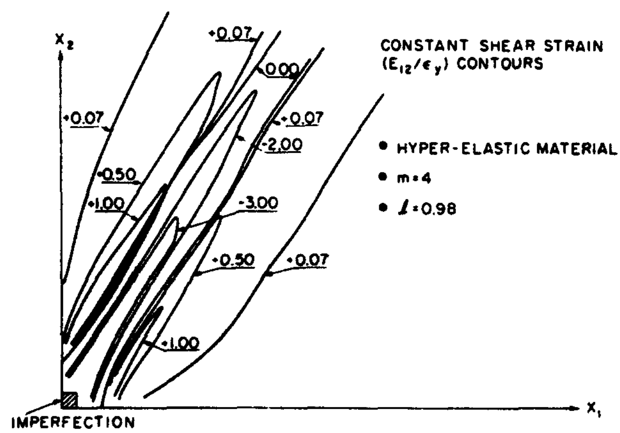

Fig. 3.

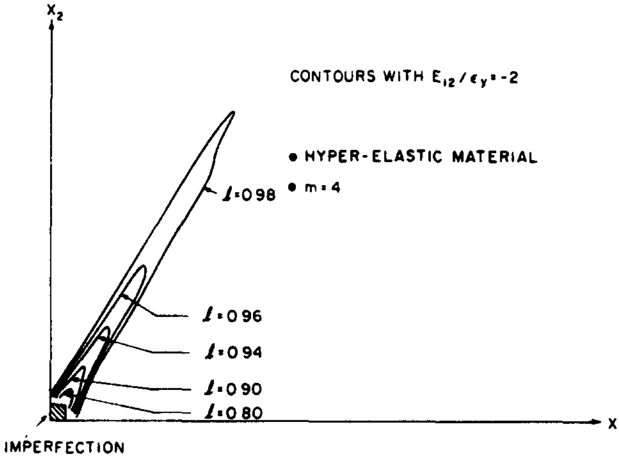

Fig. 4.

Finally, we note that because of the presence of the term β^{-1} in (3.11), and since according to (3.12) $\beta \to 0$ as $\lambda_0 \to \lambda_{cr}$, the equivalent strain ϵ_e (and similarly the shear strain E_{12}) becomes unbounded everywhere in the body (though less singularly than along the characteristic directions). This is in conflict with the assumptions made in a regular perturbation analysis and indicates that such a series solution is *not uniformly valid* with respect to λ_0. Consequently, despite the good qualitative agreement between the "solution" obtained here and experimental observations, its quantitative implications are questionable. It is of interest to determine the range of validity of the results obtained here. With this objective in mind, in the next section we solve the original nonlinear problem directly by the finite element method and compare those results with the ones here.

3.2 *Hypo-elastic material*

In this case, the functions g in (3.1) denoting the r.h.s. of (2.15) involves the unknown quantities $\bar{u}$ and $\bar{s}$. Therefore, (3.1) *does not* provide a solution to our problem and one cannot directly write down expressions for the various field quantities. If we denote the vector ($\bar{u}_1$, $\bar{u}_2$, $\bar{s}_{11}$, $\bar{s}_{22}$, $\bar{s}_{12}$, $\bar{p}$) by V, the original equations governing the hypo-elastic body are amenable to the form $\dot{V} + A(\lambda_0)[V] = f$ where A is a linear operator on V. Although a solution to this non-autonomous linear equation can be constructed (e.g. see Friedman[22]), it cannot, in general, be put into a closed form.

Nevertheless, in the special case of a "strain (or stress) induced imperfection" it is possible to exhibit the localization features of the solution *at the instant* when the imperfection appears. Such imperfections are often encountered in practice, as for example the sudden nucleation of voids in an initially homogeneous body when the strain (or stress) reaches a certain critical level. Accordingly, the imperfection amplitude $\bar{\xi} = 0$ before the appearance of the imperfection and $\bar{\xi} = \text{constant}$ ($\neq 0$) thereafter. Consequently, at the instant of appearance, the perturbed displacements $\bar{u}$ and stresses $\bar{s}$ vanish and the function g depends only on known quantities. Thus, the Lagrangian shear strain rate $\dot{\bar{E}}_{12}$ is found from (1.19), (2.12), (2.14) and (3.1) to be

$$\dot{\bar{E}}_{12} = \frac{1}{2}\int_{-\infty}^{\infty}\int_{-\infty}^{\infty} [G_{,22}(x_1 - \omega_1, x_2 - \omega_2) - G_{,11}(x_1 - \omega_1, x_2 - \omega_2)]g(\omega_1, \omega_2)\,d\omega_1\,d\omega_2 \tag{3.17}$$

where $G_{,22} - G_{,11}$ is given by

$$G_{,22}(x_1, x_2) - G_{,11}(x_1, x_2) = \frac{1}{4\pi(\alpha^2 - \beta^2)(\mu - (\sigma/2))}\left[\left(\frac{1}{\alpha} + \alpha\right)\ln(x_1^2 + \alpha^2 x_2^2) - \left(\frac{1}{\beta} + \beta\right)\ln(x_1^2 + \beta^2 x_2^2)\right] \tag{3.18}$$

when the polynomial (3.4) has four purely imaginary roots. As mentioned previously when the roots are all complex, such as in the case of a power-law material with hardening exponent $m > 2$, the localization features are similar to those of a hyper-elastic material. On the other hand, when $2 \geq m > 1$ the shear strain rate is described by (3.17), (3.18). In this case, since $\mu_{cr} = \sigma_{cr}/2$,[18], it can be shown from (3.8) that as $\lambda_0 \to \lambda_{cr}$

$$\alpha \to \frac{1}{\sqrt{2}}\left(\frac{\mu_{cr} + \sigma_{cr}/2}{2\mu^*_{cr} - \mu_{cr}}\right)^{1/2}, \quad \beta \to \infty, \tag{3.19}$$

where the subscript cr denotes evaluation at $\lambda_0 = \lambda_{cr}$.

Therefore, as $\lambda_0 \to \lambda_{cr}$ the second logarithmic term in (3.18) becomes unbounded everywhere in the (x_1, x_2)-plane except along the x_1-axis. This suggests that when a loss of ellipticity is approached, the strain field near the x_1-axis is significantly different from that elsewhere. (The characteristic direction at the instant the material becomes parabolic is, of course, the x_1-direction.)

Reconsidering the particular rectangular imperfection (3.14), it can be shown that in the limit $\lambda_0 \to \lambda_{cr}$, the shear strain rate $\dot{E}_{12}$ becomes unbounded along the two straight lines $x_2 = \pm \lambda_0^{-1} B$ which are parallel to the x_1-axis and pass through the vertices of the imperfection, whereas it remains bounded everywhere else.

A numerical example is presented in Figs. 5 and 6 for a material with hardening exponent $m = 1$, imperfection amplitude $\bar{\xi} = -0.01$ and imperfection dimensions $A/B = 1.0$. Figure 5 shows the variation of the (non-dimensional) shear strain rate $\lambda_0 \dot{E}_{12}/\epsilon_y$ along the line $X_1 = 11A$. The graph is drawn for various values of the prescribed load l. We note that the shear strain rate is negligible at small values of the load but increases dramatically in a (confined) zone near the x_1-axis as the load level approaches unity.

Figure 6 shows the contours of equal strain rate $\dot{E}_{12}\lambda_0/\epsilon_y = -1$ drawn at different load levels $l = 0.80$, 0.93, 0.97, 0.99. Here also, we observe that the influence of the imperfection is felt predominantly along the characteristic directions, the x_1-axis in this case, and that strain rate concentration becomes significant only when λ_0 is close to λ_{cr}.

4. FINITE ELEMENT SOLUTION

Here we obtain a numerical solution to the nonlinear problem posed in Section 1 by means of the finite element method. A full Lagrangian formulation of the problem is adopted, with the stress-free configuration used as the reference one and convected cartesian coordinates are employed. Material incompressibility is approximately accounted for by the introduction of a slight degree of compressibility in the material (see Needleman[23] for a more detailed discussion).

In order to simulate the boundary conditions at infinity, displacements corresponding to a

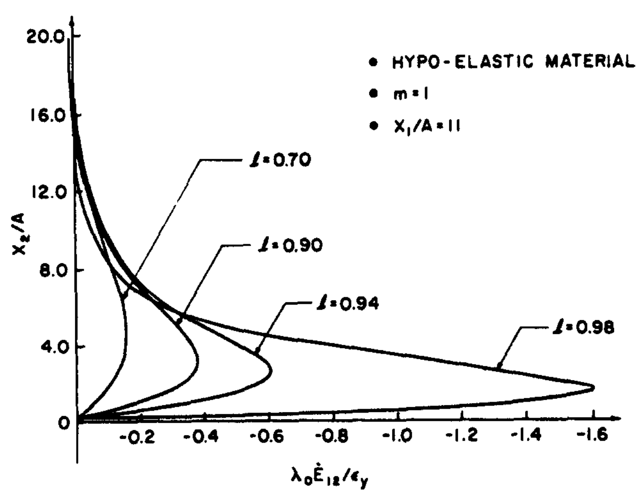

Fig. 5.

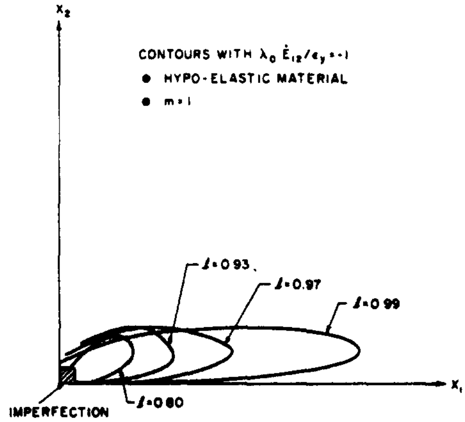

Fig. 6.

uniform state of strain ($\lambda_1 = \lambda_0$, $\lambda_2 = \lambda_0^{-1}$) are prescribed along the boundaries of the rectangle $A_1A_2A_3A_4$ (see Fig. 7). In view of the symmetry of the deformation, only the upper right rectangle $OB_1A_1B_2$ is analyzed.

The type of grid and elements used for the two constitutive models are identical. The finite element grid consists of quadrilaterals, each made up of four triangular sub-elements (formed by the two diagonals of the quadrilateral) with linear displacement fields. For each quadrilateral, static condensation is used to eliminate the nodal degrees of freedom corresponding to the center node. The choice of this particular element† was motivated by the desire to have the least possible coupling between nodes (and therefore more degrees of freedom), because of the anticipated localized form of the deformation pattern.

The rectangle $OB_1A_1B_2$ is divided into a uniform grid consisting of N elements in the X_1-direction and M elements in the X_2-direction. The dimensions of $OB_1A_1B_2$ are chosen so that the diagonal OA_1 is parallel to the characteristics of the material at the instant of loss of ellipticity, $OB_2/OB_1 = \tan\theta_{cr}$ (except in the case of a hypo-elastic material with hardening exponent $m \leq 2$, in which case we take $OB_1 = OB_2$). As observed by Tvergaard *et al.*[8], this particular mesh design leads to a very good agreement between the numerically computed directions of localization and the corresponding theoretical values.

The only difference in the finite element treatment of the two constitutive models is that in the case of a hyper-elastic material an incremental Newton–Raphson procedure is used to solve the discretized equations, while for the hypo-elastic material we adopt a straightforward incremental method.

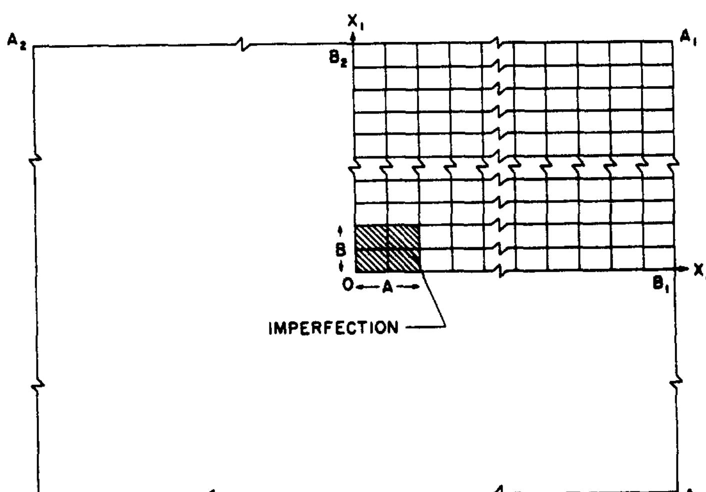

Fig. 7.

† Higher order elements tried (6 node strain triangles) for the same number of degrees of freedom gave less accurate results and were excessively time consuming.

4.1 *Hyper-elastic material*

The elastic constitutive relation employed here is similar to the one used by Hutchinson and Tvergaard[21] and Tvergaard *et al.*[8] and characterizes a material with a slight degree of compressibility. For volume preserving deformations, the limit $\nu \to 0.5$ (ν = Poisson's ratio) of this strain energy density function yields the incompressible description (1.15a) employed previously. The specific form of the strain energy density function was determined by requiring that the principal Kirchoff stresses at a given state of deformation should be identical to those in the compressible Stören-Rice material (as specified subsequently) when the latter is deformed in a path independent way under the action of the same principal stretches (see[8] and[26]).

In the finite element approximation, we seek a displacement field u in the form $u = \gamma_1 f_1(X) + \ldots + \gamma_n f_n(X)$ which minimizes the total strain energy of the body. Here γ_i are the nodal degrees of freedom of the displacement field and the shape function $f_i(X)$ are continuous and vanish at the boundary of the body. Accordingly, the nonlinear algebraic equations of the discretized problem to be solved in order to determine γ_i are

$$\int_A \frac{\partial W}{\partial \gamma_j}\,\mathrm{d}A = \int_A \frac{\partial W}{\partial E_{\alpha\beta}}\frac{\partial E_{\alpha\beta}}{\partial \gamma_j} = \int_A s_{\alpha\beta}\frac{\partial E_{\alpha\beta}}{\partial q_j}\,\mathrm{d}A = 0. \tag{4.1}$$

A Newton–Raphson scheme is used to iteratively solve these equations. A more detailed discussion may be found in [26].

4.2 *Hypo-elastic material*

For the case of a Stören–Rice material the path dependence of the solution must be taken into account. This is done by a straightforward linear incremental method based on the principle of virtual work

$$\int_A [L_{\alpha\beta\gamma\delta}\dot{E}_{\alpha\beta}\delta\dot{E}_{\gamma\delta} + s_{\alpha\beta}\dot{u}_{\epsilon,\alpha}\delta\dot{u}_{\epsilon,\beta}]\,\mathrm{d}A = 0. \tag{4.2}$$

It is understood that the admissible velocity fields in (4.2) will have to satisfy the zero velocity boundary condition.

The incremental moduli corresponding to the slightly compressible version of the Stören and Rice material are given in[26]. Here we note that for deformation histories in which the principal axes of strain remain fixed with respect to the material, the model is path independent and a strain energy function coinciding with the one in Section 4.1 exists. The linear incremental procedure used, is in fact a special case of the iterative method described previously for the hyper-elastic material. In order to ensure the accuracy of the solution, small increments must be taken. At each increment, the values of the second Piola–Kirchoff stress components at every sub-element as well as the nodal displacements need to be stored in order to start the next step.

The increment size for the calculations were chosen as follows: The program was first run with only one element and with the desired values of the various parameters using various step sizes. The largest increment size which computed the stresses to within an error of 0.1% was then chosen for all further calculations.

5. NUMERICAL RESULTS

In this section we compare the results of the finite element calculations with the analytical predictions of the linearized model. All the results reported here are obtained using a yield strain $\epsilon_y^0 = 0.001$ (which is of an order typical for most structural metals). For this value of the yield strain, numerical experimentation indicates that the results, for hardening exponents $m > 1$, are almost insensitive to the Poisson ratio ν in the range 0.3–0.495, and in all subsequent calculations we take $\nu = 0.49$.

For a load range $l = 0.0$–0.995 and for distances from the imperfection $R/A \geq 5.0$, three different values of the imperfection amplitude parameter $\bar{\xi}$ were considered ($\bar{\xi} = -0.04$, -0.01

and -0.0025). In all cases it was found that the shear strain E_{12} depended almost linearly on $\bar{\xi}$ and consequently, only the results for the case $\bar{\xi} = -0.01$ will be presented here.

We also mention that throughout the finite element computations, the sides of the rectangle $OB_1A_1B_2$ (see Fig. 7) are taken to be $OB_1 = 20A$ and $OB_2 = 20B$ where $2A$ and $2B$ are the undeformed imperfection dimensions (in the X_1- and X_2-direction respectively).

All results are presented with reference to the unloaded configuration, with (R, Θ) being polar coordinates centered at the origin. Note that in this configuration, the inclination of the characteristics to the X_1-axis at the instant of loss of ellipticity are $\pm\Theta_{cr}$ where

$$\tan \Theta_{cr} = \lambda_{cr}^2 \tan \theta_{cr}, \tag{5.1}$$

with θ_{cr} given by (2.10) for the hyper-elastic material and (2.19) for the hypo-elastic one.

5.1 *Hyper-elastic material*

Figure 8(a) shows the angular variation of the nondimensional shear strain E_{12}/ϵ_y along a circular arc of radius $R = 15\,A$ centered at the origin. The graphs are drawn for various values of the applied load, $l = 0.7$, 0.9, 0.94 and 0.98, where the load l is related to the applied stretch λ_0 by (3.16). The results displayed are for a material with hardening exponent $m = 4$ for which we have from (2.10), (2.11) and (5.1) that $\lambda_{cr} \simeq 1.685$, $\theta_{cr} \simeq 59.3°$. The solid line represents the theoretical predictions based on the perturbation analysis while the dashed line represents the numerical results for a 20×20 finite element grid. Figure 8(b) compares the same theoretical results with finite element calculations using a 40×40 grid.

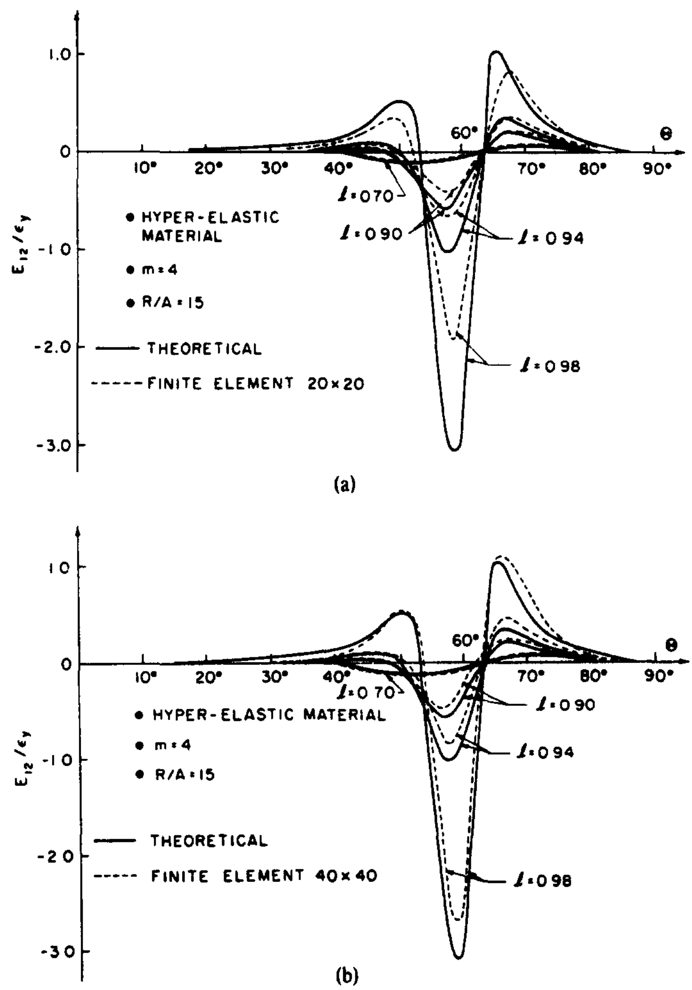

Fig. 8.

We observe that for loads l as high as $l = 0.9$, the finite element results for both meshes are in good agreement with the theoretical predictions, presumably since very little localization occurs at this load level. At higher loads, $l = 0.94$, 0.98, the finite element results in Fig. 8(a) follow the trend of the theoretical curves but become increasingly inaccurate around the strain peaks. The 40×40 mesh in Fig. 8(b) shows considerably better agreement, even at loads as high as $l = 0.98$.

One does not, of course, expect the theoretical results to be uniformly accurate at all points in the body. In Fig. 9 we have plotted, for the same material, the angular variation of E_{12}/ϵ_y along a circular arc of radius $R = 5A$, in the case of a 40×40 element mesh. On comparison with Fig. 8(b), we observe that the error in this case, particularly near the peaks, is greater than that on the arc $R = 15A$ at the same load. This is especially visible near the right upward peak at a load $l = 0.98$. This suggests, as one might have expected, that the theoretical results become increasingly accurate (at least relative to the finite element results) as one moves away from the imperfection.

In order to examine the variation of strain with distance from the imperfection, in Fig. 10 we plot the (theoretical) angular variation of E_{12}/ϵ_y along a number of circular arcs at the same load $l = 0.997$. We see that on the arc $R = 5A$ a fairly wide zone is affected by the imperfection (roughly $30° < \Theta < 85°$) and that the downward peak suddenly narrows and becomes exceedingly sharp in the vicinity of $\Theta = 59°$ ($\simeq \Theta_{cr}$). As we move away from the imperfection, say at

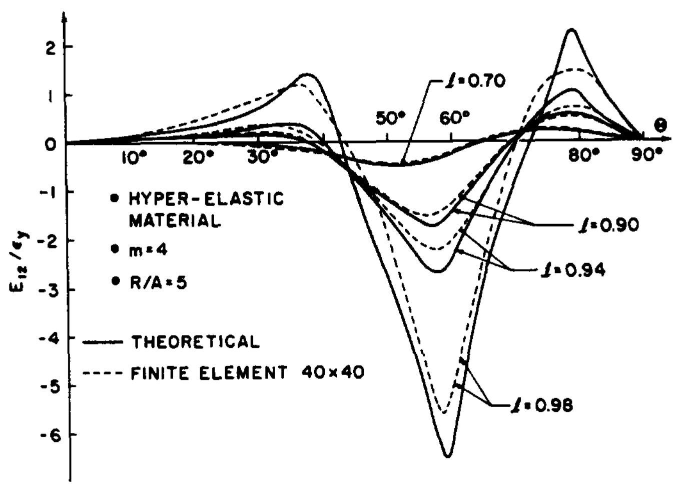

Fig. 9.

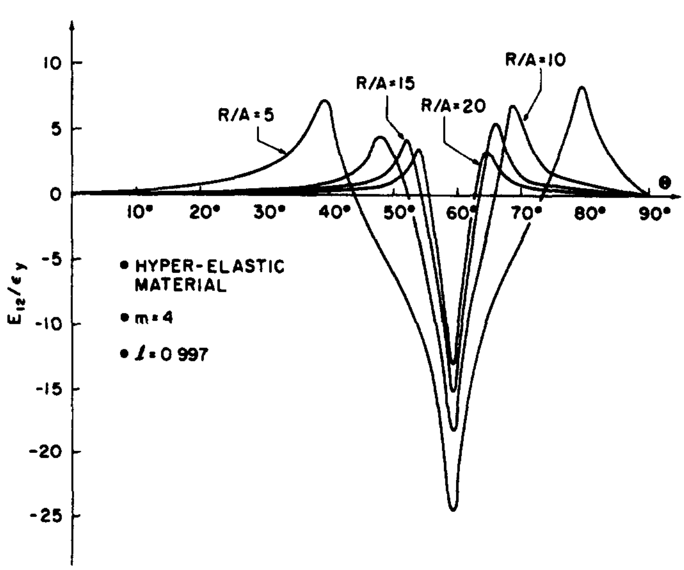

Fig. 10.

$R = 20A$, the zone which is disturbed by the imperfection becomes noticably narrower (roughly $50° < \Theta < 70°$) and the downward peak is somewhat more rounded. As anticipated, the magnitude of the shear strain decreases as the distance from the imperfection increases. Note that in all cases the maximum shear strain occurs almost exactly at the theoretically predicted angle.

Finally, in order to study the effect of the hardening exponent m on the solution, we plot the angular variation of shear strain E_{12}/ϵ_y for different values of m at a distance $R = 15A$ from the center of the imperfection. Figure 11 shows these curves for $m = 2$, 4 and 10 at a load level $l = 0.98$. The peaks are seen to occur very close to the theoretically† predicted angle and the associated value of shear strain decreases considerably (from $E_{12}^{max} \simeq 11\epsilon_y$ for $m = 2$ to $E_{12}^{max} \simeq 0.8\epsilon_y$ for $m = 10$) with increasing values of the hardening exponent. Numerical calculations performed in the cases $m = 2$, 10 with a 40×40 grid showed an agreement similar to that found in the case $m = 4$.

5.2 *Hypo-elastic Material*

In Fig. 12, we have plotted the theoretical shear strain rate $\lambda_0 \dot{E}_{12}/\epsilon_y$ vs Θ along a circular arc of radius $R = 15A$, using (3.17) and (3.5). The figure drawn corresponds to a material with hardening exponent $m = 4$. It is observed that for loads less than about $l = 0.8$, the shear strain rate is negligible. Thereafter, it begins to increase sharply within a narrow zone on either side of $\Theta \simeq 51°$. On comparison with the corresponding figure for the hyper-elastic material (Fig. 2), we notice a striking similarity, which in view of the remarks made in Section 3.2 is hardly surprising. Of course, the specific values of the angles of localization are different; in this case we find from (2.19), (2.20) and (5.1) that $\lambda_{cr} \simeq 1.542$ and $\Theta_{cr} \simeq 50.9°$.

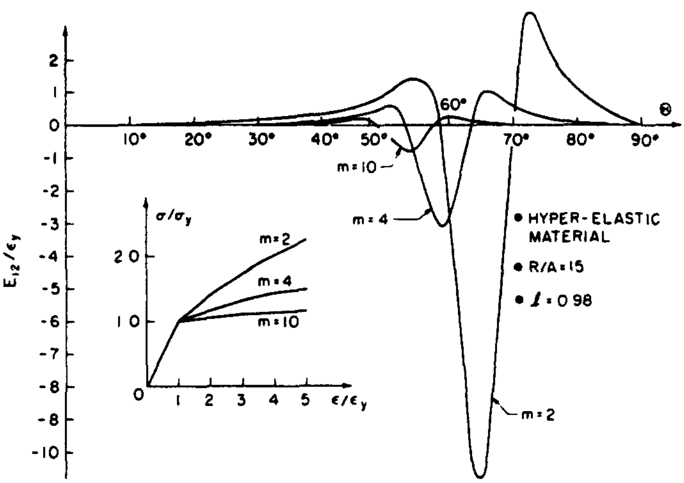

Fig. 11.

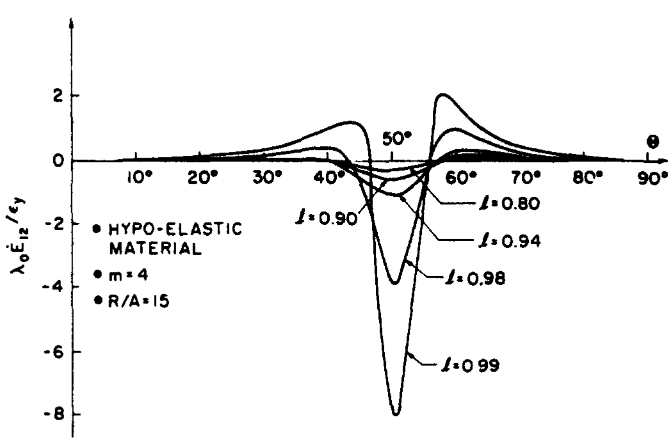

Fig. 12.

†From (2.10), (2.11) and (5.1) we find that $\lambda_{cr} \simeq 2.163$, $\Theta_{cr} \simeq 65.2°$ for $m = 2$ and $\lambda_{cr} \simeq 1.379$, $\Theta_{cr} \simeq 54.1°$ for $m = 10$

Recall from the discussion in Section 3.2 that the analytical results hold only at the instant of appearance of a strain induced imperfection. Therefore, the curve corresponding to a load level l in Fig. 12 shows the angular variation of the shear strain rate when the imperfection appeared at that particular load, in a material which was previously homogeneous.

Since the effect of an imperfection is not important until the load approaches its critical value, one expects that the particular load at which the imperfection was induced (provided that it is not close to the critical one) does not significantly affect the strain pattern at the later stages of deformation. In order to examine this hypothesis, we performed the following finite element calculations using a 20×20 grid. For a hypo-elastic material with $m = 4$ we activated the rectangular imperfection (3.14) at two different load levels $l = 0.7$ and 0.8 and computed the shear strains at subsequent loads. The agreement between the two cases were reasonably good, and the results are described in some detail in [26]. It should be remarked that the magnitudes of the shear strains were considerably less for the hypo-elastic material than for the hyper-elastic one (at the same load level), whereas the width of the band was roughly the same. Since in the path dependent material it is the strain rates that localize, the strains, which are their integrals over the deformation history, are necessarily less than those in the hyper-elastic case. On the other hand, the width of the band is set by the dimensions of the imperfection, independently of the particular constitutive law.

Finally we mention that for both constitutive models, the equivalent strain difference $\epsilon_e - \epsilon_e^0$ also showed localization effects very similar to that of the shear strain E_{12}.

6. DISCUSSION

Although the linearized model discussed in this paper is perhaps too simple to give quantitatively good results, it nevertheless predicts some of the important qualitative features relating to shear localization that are observed experimentally. It shows that up to rather high levels of strain, the effect of an imperfection is negligibly small, with its influence being essentially confined to a small region around it. As a certain critical value of strain is approached, the imperfection more or less suddenly becomes "activated" and causes a dramatic concentration of strain along narrow bands emanating from the imperfection. The width of these zones is essentially set by the dimensions of the imperfection and the bands rapidly propagate through the body as the load increases. The strain field elsewhere, continues to be relatively unaffected by the imperfection.

The critical strains involved here are those associated with a loss of ellipticity, while the directions of the shear bands are the associated characteristic directions. In this example, the imperfection-free body loses ellipticity when the applied stretch $\lambda_0 = \lambda_{cr}$. Presumably, the imperfect body loses ellipticity, locally near the imperfection, when $\lambda_0 = \lambda^*_{cr}$ where λ^*_{cr} is a number close to $\lambda_{cr}(\lambda^*_{cr} < \lambda_{cr})$. It seems likely that the activation of the imperfection and the beginning of localization occurs when $\lambda_0 = \lambda^*_{cr}$; as λ_0 is increased further, the localized zone propagates until a fully developed band forms when $\lambda_0 = \lambda_{cr}$.

The particular choice of constitutive equation and material parameters dictates the strain level at localization and also the orientation of the shear bands. However, both models studied here show the same essential features discussed above, suggesting that similar behavior may be exhibited by other constitutive models also, provided the associated incremental equilibrium equations lost ellipticity. Similarly, though our results do not describe the more interesting types of imperfections such as voids and rigid inclusions, one expects that an appropriate analysis in these cases would also show the same qualitative behavior.

It should be mentioned that there is a certain formal similarity between the analysis here and the classical bifurcation analysis of elastic (or elastic–plastic) solids Budiansky[24], Hutchinson[25]), for example, the regular perturbation expansion with respect to the imperfection amplitude and its non-validity near the critical load. We emphasize however, that the localization behavior observed here is due to a loss of ellipticity of the governing equations while the features of the behavior near the buckling load are associated with a loss of uniqueness which usually occurs within the elliptic regime.

Based on the above observations, the following mechanism for the emergence of shear bands seems plausible: near points of imperfection in the material, and after the remotely applied loading reaches a certain level, the strains start rapidly concentrating along two preferential directions. It is then possible, that the high strain concentration causes some mechanical damage at points along these directions (e.g. grain boundary separation, dislocation accumulation), which in turn act as new sources of imperfections, thus driving the phenomenon even further.

Acknowledgements—The authors wish to express their sincere appreciation to Professors A. Needleman, J. R. Rice (Division of Engineering) and C. Dafermos (Division of Applied Mathematics) for many useful discussions during the course of this study. This work was supported by the N.S.F. Materials Research Laboratory and the Division of Engineering at Brown University. The computations reported here were carried out on the VAX-11/780 computer at the Division of Engineering, Brown University. The acquisition of this computer was made possible by grants from the U.S. National Science Foundation, the General Electric Foundation and the Digital Equipment Corp.

REFERENCES

1. A. Nadai, *Theory of Flow and Fracture of Solids*, Vol. 1. McGraw-Hill, New York (1960).
2. R. Hill, Acceleration waves in solids. *J. Mech. Phys. Solids* **10**, 1–16 (1962).
3. T. Y. Thomas, *Plastic Flow and Fracture in Solids*. Academic Press, New York (1961).
4. J. W. Rudnicki and J. R. Rice, Conditions for the localization of deformation in pressure-sensitive dilatant materials. *J. Mech. Phys. Solids* **23**, 371–394 (1975).
5. J. R. Rice, The localization of plastic deformation. *Proc. 14th IUTAM Cong.* (Edited by W. T. Koiter), Delft, The Netherlands. North Holland, Amsterdam (1976).
6. J. K. Knowles and Eli Steinberg, On the failure of ellipticity and the emergence of discontinuous deformation gradients in plane finite elastostatics. *J. Elasticity* **8**, 329–379 (1978).
7. J. R. Fisher, Private communication.
8. V. Tvergaard, A. Needleman and K. K. Lo, Flow localization in the plane strain tensile test. Brown University Tech. Rep. (1980).
9. R. Hill, The essential structure of constitutive laws for metal composites and polycrystals. *J. Mech. Phys. Solids* **15**, 79–95 (1967).
10. J. W. Hutchinson, Elastic-plastic behavior of polycrystalline metals and composites. *Proc. R. Soc.* **A319**, 247–272 (1970).
11. T. H. Lin. Physical theory of plasticity. In *Advances in Applied Mechanics* (Edited by C-S. Yih), Vol. 11, pp. 255–311. Academic Press, New York (1971).
12. S. Stören and J. R. Rice, Localized necking in thin sheets. *J. Mech. Phys. Solids* **23**, 421–441 (1975).
13. L. Anand and W. Spitzig, Initiation of localized shear bands in plane strain. *J. Mech. Phys. Solids* **28**, 113–128 (1980).
14. A. E. Green and W. Zerna, *Theoretical Elasticity*. Clarendon Press, Oxford (1954).
15. B. Budiansky, Remarks on theories of solid and structural mechanics. In *Problems of Hydrodynamics and Continuum Mechanics* (Edited by M. A. Lavrent'ev), pp. 77–83. SIAM, New York (1969).
16. R. C. Abeyaratne, Discontinuous deformation gradients in plane finite elastostatics of incompressible materials. *J. Elasticity* 10 (1980).
17. C. Truesdell, Hypo-elasticity. *J. Rat. Mech. Anal.* **4**, 83–133 (1955).
18. R. Hill and J. W. Hutchinson, Bifurcation phenomena in the plane tension test. *J. Mech. Phys. Solids* **23**, 239–264 (1975).
19. M. J. Lighthill, *Fourier Analysis and Generalized Functions*. Cambridge Univ. Press (1958).
20. I. M. Gel'fand and G. E. Shilov, *Generalized Functions*, Vol. 1. Academic Press, New York (1964).
21. J. W. Hutchinson and V. Tvergaard, Surface instabilities on statically strained plastic solids. *Harvard Univ. Technical Report* (1979).
22. A. Friedman, *Partial Differential Equations*. Krieger, New York (1976).
23. A. Needleman, Numerical study of necking of circular cylindrical bars. *J. Mech. Phys. Solids* **20**, 111–127 (1972).
24. B. Budiansky, Theory of buckling and post-buckling behavior of elastic structures. In *Advances in Applied Mechanics* (Edited by C-S. Yih), Vol. 14, pp. 1–65 (1974). Academic Press, New York.
25. J. W. Hutchinson. Plastic buckling. In *Advances in Applied Mechanics* (Edited by C-S. Yih), Vol. 14, pp. 66–143. Academic Press, New York (1974).
26. R. Abeyaratne and N. Triantafyllidis, On the emergence of shear bands in plane strain. Brown University Tech. Rep. *MRL E*-125 (July 1980).